Applied Catalysis B: Environmental 212 (2017) 68–79

Contents lists available at ScienceDirect

Applied Catalysis B: Environmental

journal homepage: www.elsevier.com/locate/apcatb

Enhanced catalytic activity of Ni on η-Al_2O_3 and ZSM-5 on addition of ceria zirconia for the partial oxidation of methane

Ahmed I. Osman[a,b], Jonathan Meudal[c], Fathima Laffir[d], Jillian Thompson[a,*], David Rooney[a,*]

[a] School of Chemistry and Chemical Engineering, Queen's University Belfast, Belfast BT9 5AG, Northern Ireland, UK
[b] Chemistry Department, Faculty of Science–Qena, South Valley University, Qena 83523, Egypt
[c] ENSICAEN, 6 Boulevard Maréchal Juin, 14000 Caen, France
[d] Department of Chemical and Environmental Sciences, Materials and Surface Science Institute, University of Limerick, Limerick, Ireland

ARTICLE INFO

Article history:
Received 8 September 2016
Received in revised form
28 November 2016
Accepted 23 December 2016
Available online 2 January 2017

Keywords:
Methane
Partial oxidation
Zeolite support
Oxygen carrier
Nickel
CeO_2-ZrO_2

ABSTRACT

Nickel supported on η-Al_2O_3 and ZSM-5(80) catalysts with and without the addition of ceria-zirconia, were prepared by co-precipitation and wet impregnation methods and used for the low temperature catalytic partial oxidation of methane (CPOM). The catalysts were tested under reaction temperatures of between 400 and 700 °C with a WHSV of 63,000 mL g^{-1} h^{-1}. The activity of the catalyst was found to be dependent on the support and preparation method. The optimum catalyst composition of those tested was 10% Ni on 25%CeO_2-ZrO_2/ZSM-5(80), prepared by co-precipitation, where the reaction reached equilibrium conversion at 400 °C ($T_{50\%}$ < 400 °C), which is one of the lowest temperatures reported to date. Further increases in temperature led to improved selectivity to CO reaching 60% at 600 °C. Although the observed kinetics were found to be controlled by strong adsorption of CO at lower temperature, this was an equilibrium limitation with longer time on stream experiments showing no decrease in the catalyst activity over 25 h at 400 °C.

1. Introduction

Methane which is obtained from natural gas or biological sources, is a valuable energy resource and chemical feed stock [1,2]. While its complete combustion generates a large amount of energy, CO_2 and water [3] partial combustion results in a mixture of gases including CO and H_2, syngas, which is a building block for higher hydrocarbons.

In general, syngas is formed by the large scale steam reforming of hydrocarbons and used for a variety of applications including the manufacture of fuels, feedstocks and the production of hydrogen [4]. Scaling down such processes to utilise stranded and small scale sources of methane is desired as is the development of catalysts which allow partial oxidation of methane to syngas under milder conditions [5]. This is particularly required as at high processing temperatures (>800 °C) coke formation is thermodynamically favoured reducing the yield of syngas [5–7]. In addition, depending on the source of the gas and oxidant used, nitrogen oxides (NO_x) and sulfur oxides (SO_x) as well as particulates can be formed with associated health and environmental impacts [8]. Overall, working at lower temperatures offers significant financial and environmental advantages, including lower energy and materials costs as well as reduced formation of pollutants. The aim of this work is to develop a catalyst that can facilitate CPOM at low temperatures yet still gives high selectivity.

To date various catalysts have been reported for CPOM such as Rh, Ru, Pd, Pt and Ir as well as less expensive metals such as Ni and Co [1,5,9]. Nickel is recognised as being one of the most active and least expensive, however, it is susceptible to poisoning by carbon deposition [10]. To ameliorate this, reducible oxide supports such as TiO_2, La_2O_3, CeO_2, ZrO_2 as either single supports or in combination have been used in many high temperature reactions as the labile oxygen in the support is able to oxidize and remove any coke formed [11–17]. In addition to this, the strong metal-support interaction often improves the activity of these catalysts [18].

For example de Abreu et al. [14] showed that during steam reforming over Ni supported on a mixed oxide of Al_2O_3 with different ratios of CeO_2 and ZrO_2 improved activity and stability to coke was obtained with higher ratios of CeO_2. Scarabello et al. [13] reported a higher activity, as evidenced by a 60 °C reduction in ignition temperature, for partial methane oxidation on addition

* Corresponding authors at: Corresponding School of Chemistry and Chemical Engineering, Queen's University Belfast, David Keir Building, Stranmillis Road, Belfast BT9 5AG, Northern Ireland, UK.
E-mail addresses: jillian.thompson@qub.ac.uk (J. Thompson), d.rooney@qub.ac.uk (D. Rooney).

http://dx.doi.org/10.1016/j.apcatb.2016.12.058
0926-3373/

of CeO_2 to 0.5 wt% Rh/ZrO_2. In these multi-component catalysts, the component ratio, as well as their mutual interactions, all affect the observed rate and selectivity. Pantaleo et al. [6] showed that the method of Ni deposition as well as support composition both affected the observed activity. Here Ni deposited by wet impregnation on La_2O_3 or CeO_2/La_2O_3 gave a range of nickel/lanthanum oxides and improved activity compared to those prepared by co-precipitation. However, in contrast, catalysts prepared by co-precipitation on CeO_2 alone gave smaller crystallites and lower combustion temperatures than those prepared by wet impregnation. The most active catalysts gave a 50% conversion ($T_{50\%}$) at around 675 °C using a weight hourly space velocity (WHSV) of 60,000 mL g^{-1} h^{-1}. Larimi et al. tested Ni catalysts supported on different compositions of CeO_2/ZrO_2 and also found increased activity with increasing ZrO_2 in the support. The most active catalyst gave similar results to those obtained by Pantaleo et al. a $T_{50\%}$ of 550 °C and CO selectivity of 90% at 750 °C [19].

However, a limitation of using many of these reducible mixed oxides, such as CeO_2-ZrO_2 and CeO_2/La_2O_3 as supports is their inherently low surface area and high cost. To overcome this a mixed support of Al_2O_3, as an inexpensive high surface area support, and reducible oxide such as CeO_2-ZrO_2 for its redox properties, is often used for high temperature catalysis [16,18]. Dajiang et al. used a combined support of CeO_2-ZrO_2 with Al_2O_3 and found a significant increase in the catalytic activity for Ni/CeO_2-ZrO_2-Al_2O_3 which was attributed to the increased surface area of 165.3 m^2 g^{-1} compared with 25.8 m^2 g^{-1} for the catalyst without Al_2O_3. In this case a $T_{90\%}$ at approximately 720 °C was obtained for the mixed oxide catalyst [16].

Close contact of the Ni and the reducible oxide support is however needed to provide a good interaction of the Ni with the oxygen vacancies on the support. This not only improves the redox behaviour of the Ni during the catalytic cycle but also helps supply oxygen to facilitate removal of any coke deposited. This can be achieved by preparing catalysts with very small particle sizes or by preparing the catalysts by co-precipitation.

Xu et al. showed that preparation of 10 wt% Ni on single and mixed CeO_2/ZrO_2 supports by co-precipitation resulted in an improved interaction between the catalyst components and improved activity was observed. A $T_{50\%}$ of 525 °C was obtained for the Ni/CeO_2 catalyst prepared by co-precipitation compared to around 630 °C for the catalyst prepared by impregnation at WHSV of 10,400 mL g^{-1} h^{-1} [17].

Cai et al. [18] examined Ni on Al_2O_3, ZrO_2-Al_2O_3, CeO_2-Al_2O_3 and CeO_2-ZrO_2-Al_2O_3 prepared by coprecipitation for methane auto-thermal reforming. Here the Ni/CeO_2-ZrO_2-Al_2O_3 was the best amongst those studied with a $T_{50\%}$ around 600 °C and $T_{90\%}$ at 750 °C at a GHSV of 4800 h^{-1}. This improvement of the catalytic performance on addition of CeO_2-ZrO_2 was attributed to increased dispersion of NiO thus improving oxygen transfer but also decreasing the formation of nickel aluminate. These works confirm that the combination of Ni, a high surface area support and oxygen carrier can result in improved activity at low temperatures. However, to date, a full investigation of these has not been conducted.

Currently, two main mechanisms have been reported for CPOM. The direct partial oxidation (DPO) mechanism involves the dissociation of methane followed by oxidation of surface carbon to CO and subsequent desorption of CO and H_2 gases. The combustion and reforming reaction (CRR) mechanism involves the complete combustion of methane to CO_2 and H_2O which are then converted through reforming to CO and H_2. For a given catalyst the precise mechanism is likely to be dependent on a number of factors including metal, support and reaction conditions [20–27]. Of these the DPO mechanism is similar to that reported for the palladium catalysed total methane oxidation (TMO) reaction where the methane dissociatively adsorbs on the metal and the methyl species are then fully oxidized by PdO present on the surface. The resulting reduced metal species are then reoxidised by the gas phase oxygen [28]. Recently we have reported the low temperature total oxidation of methane over a Pt/Pd bimetallic catalyst supported on a dual support of a zeolite and TiO_2. In that work the zeolite acidity assists in activating the methane as well as enhancing the reoxidation of the Pd(0) while the titania increases oxygen transport to the active Pd metal [29]. Given the similarities between the mechanisms of the TMO and DPO reactions along with the recent report of a Ni/beta zeolite catalyst showing high activity and stability for CPOM [30] a similar catalyst design to that used for the low temperature TMO was proposed to study CPOM.

Herein Ni was supported onto η-Al_2O_3, ZSM-5(80) and CeO_2-ZrO_2 as well as a combination of supports, namely CeO_2-ZrO_2-Al_2O_3 and CeO_2-ZrO_2-ZSM-5(80), prepared by either co-precipitation or wet-impregnation methods. As in the case of the TMO reaction the zeolite was used to activate the methane and improve the reoxidation of the Ni, CeO_2/ZrO_2 is used for oxygen mobility, improving redox behaviour and oxidation of any deposited carbon. Co-precipitation was also used to optimise the interaction of the catalyst components. These catalysts were characterised and tested for partial oxidation of methane at a realistic WHSV of 63,000 mL g^{-1} h^{-1}.

2. Experimental

2.1. Materials

The chemicals used in the present study were all of analytical grade and were used without further purification. Aluminium nitrate nonahydrate (≥98%), ammonia solution (35%), ammonium cerium(IV) nitrate (≥98.5%), zirconium(IV) oxynitrate hydrate (99%), cerium(IV)-zirconium(IV) oxide ($Ce_{0.5}Zr_{0.5}O_2$) nanopowder <50 nm particle size (99%) ($CeZr^{Com}$) and nickel(II) nitrate hexahydrate (99.999%) were all obtained from Sigma-Aldrich. Zeolite H-ZSM-5(80) (SiO_2:Al_2O_3 80:1 mol ratio) was obtained from Alfa Aesar. All gases, Ar, CH_4, O_2/Ar and Ne were obtained at 100% purity from BOC gases, UK.

2.2. Catalyst preparation

2.2.1. Preparation of the supports

The preparation of the η-alumina support has been described in a previous work [31]. After precipitation of the aluminium nitrate precursor by ammonia solution, the resulting precipitate was calcined at 550 °C. $Ce_{0.5}Zr_{0.5}O_2$ ($CeZr^{Com}$) and H-ZSM-5(80) were used as received.

CeO_2-ZrO_2 supports prepared by co-precipitation (CeZr-CP) were prepared by mixing the appropriate amount of ammonium cerium(IV) nitrate and zirconium(IV) oxynitrate hydrate with 35 wt% ammonia solution that was added dropwise under vigorous stirring (pH ~10) at a temperature of 80 °C. The precipitate was aged for 2 h while stirring at 80 °C before being removed by filtration, washed with deionised water, dried at 120 °C for 12 h and calcined at 600 °C for 6 h at a heating rate of 2 °C min^{-1}. The CeO_2-ZrO_2-Al_2O_3 prepared by co-precipitation (CeZrAl-CP) and CeO_2-ZrO_2-ZSM-5(80) prepared by co-precipitation (CeZrZ-CP) were prepared in the same way as described above for the CeZr-CP support except that the appropriate amount of aluminium nitrate nonahydrate or zeolite respectively was mixed with ammonium cerium(IV) nitrate, zirconium(IV) oxynitrate hydrate and the 35 wt% ammonia solution.

CeZrAl-WI supports were prepared by placing η-Al_2O_3 in a vial with the appropriate amount of $Ce_{0.5}Zr_{0.5}O_2$ ($CeZr^{Com}$) and mixing with deionized water (5 mL). The mixture was sonnicated at 80 °C

(Crest ultrasonic bath model 200 HT), at 45 kHz frequency for 3 h resulting in a homogeneous paste which was then dried at 120 °C overnight. CeZrZ-WI supports were prepared in the same way as that described for CeZrAl-WI except that the η-Al_2O_3 was replaced with H-ZSM-5(80).

2.2.2. Preparation of nickel on η-Al_2O_3, H-ZSM-5(80), CeZr, CeZrAl and CeZrZ supports

Nickel catalysts were prepared by a wet impregnation method with the aid of sonnication. The pure supports η-Al_2O_3, H-ZSM-5(80), CeZr-CP or the CeZrAl or CeZrZ prepared by either WI or CP methods were placed in a vial and the mass of metal precursor solution, $Ni(NO_3)_2{\cdot}6H_2O$ in deionised water (5 mL) required to give a 10 wt% nickel loading was added to the powder. The mixture was sonnicated at 80 °C (Crest ultrasonic bath model 200 HT), at 45 kHz frequency for 3 h resulting in a homogeneous paste. All mixtures were dried at 120 °C overnight before being calcined in air at 550 °C for 4 h with a heating ramp of 2 °C min^{-1}. These catalysts were used for all reactions. A sample of each catalyst was also calcined at 700 °C for surface area analysis.

Seven catalysts with the compositions given below were prepared to determine the effect of the preparation method and support. Each catalyst contained 10 wt% Ni.

- NiAl: 90% η-Al_2O_3
- NiZ: 90% ZSM-5(80)
- NiCeZr-CP: 90% $Ce_{0.5}Zr_{0.5}O_2$ ($(NH_4)_2Ce(NO_3)_6 + ZrO(NO_3)_2{\cdot}xH_2O$)
- NiCeZrAl-CP: 25% $Ce_{0.5}Zr_{0.5}O_2$ ($(NH_4)_2Ce(NO_3)_6 + ZrO(NO_3)_2{\cdot}xH_2O$) + 65% η-$Al_2O_3$
- NiCeZrAl-WI: 25% $Ce_{0.5}Zr_{0.5}O_2$ ($CeZr^{Com}$) + 65% η-Al_2O_3
- NiCeZrZ-CP: 25% $Ce_{0.5}Zr_{0.5}O_2$ ($(NH_4)_2Ce(NO_3)_6 + ZrO(NO_3)_2{\cdot}xH_2O$) + 65% ZSM-5(80)
- NiCeZrZ-WI: 25% $Ce_{0.5}Zr_{0.5}O_2$ ($CeZr^{Com}$) + 65% ZSM-5(80)

2.3. Catalyst characterization

Powder X-ray diffraction (XRD) was carried out using a PANalytical X'Pert Pro X-ray diffractometer. This diffractometer was equipped with a CuK_α X-ray source with a wavelength of 1.5405 Å. The diffractograms were collected up to 2θ = 80°. The X-ray tube was set at 40 kV and 40 mA. Peaks were selected and compared to diffraction patterns in the software library.

Brunauer-Emmett-Teller (BET) analysis was performed using a Micromeritics ASAP 2020 system. BET surface area and pore volume were measured by N_2 adsorption and desorption isotherms at liquid nitrogen temperature (−196 °C).

Temperature-programmed reduction (TPR) was determined using a Micromeritics Autochem 2910 apparatus. The sample (0.1 g) was placed in a quartz tube under flowing Ar before reduction using 5% H_2/Ar with a flow rate 30 mL min^{-1} until a stable baseline was obtained. The sample was then heated at 10 °C min^{-1} up to 700 °C and the H_2 uptake monitored by a TCD.

TPO data were obtained on a PX200, Tianjin Pengxiang Sci. & Tech. Co., China apparatus. The sample (0.1 g) was placed in a quartz tube under He for 10 min, followed by heating to 200 °C at 15 °C min^{-1}. After 30 mins the temperature was decreased to 25 °C at 5 °C min^{-1}. A flow of 10% O_2 in Ar at 30 mL min^{-1} was passed over the catalyst until a stable baseline was obtained before being heated at 10 °C min^{-1} up to 700 °C with the O_2 uptake monitored by a TCD.

Determination of the concentration of Lewis and Brönsted acid sites on the synthesized catalysts was performed by Diffuse Reflectance Infrared Fourier Transform (DRIFT) spectroscopy of adsorbed pyridine using a Bruker Vertex 70 FTIR Spectrometer equipped with a liquid N_2-cooled MCT detector. Samples were pre-treated by outgassing at 120 °C for 30 mins under an Ar atmosphere. Samples were then saturated with pyridine in-situ at 50 °C for 30 min using an Ar stream (flow rate 15 mL min^{-1} and reservoir at room temperature), with the physisorbed pyridine removed by flushing at 50 °C with Ar gas for 30 mins. DRIFTS analysis was carried out at 40 °C at a resolution of 4 cm^{-1} and an accumulation of 56 scans every 30s. Spectra of the fresh samples (before pyridine adsorption) were subtracted to observe the bands corresponding to the adsorbed pyridine and in turn the Lewis and Brönsted acidic sites on the supports.

Scanning Electron Microscopy (SEM) was carried out on a FEI Quanta 250 FEG MKII with a high resolution environmental microscope (ESEM) using XT Microscope Control software and linked to an EDX detector. The EDX used was a 10 mm^2 SDD Detector-x-act from Oxford Instruments which utilizes Aztec® EDS analysis software. Both systems used the same chamber.

XPS was performed in a Kratos AXIS Ultra instrument using a monochromated Al Kα radiation of energy 1486.6 eV. High resolution spectra of Ce 3d, Ni 2p, Zr 3d and O 1s were taken at fixed pass energy of 20 eV, 0.05 eV step size and 100 ms dwell time per step. Surface charge was efficiently neutralised by flooding the sample surface with low energy electrons. Core level binding energies were corrected using the C 1s peak at 284.8 eV as charge reference. For construction and fitting of synthetic peaks of high resolution spectra, a mixed Gaussian-Lorentzian function with a Shirley type background subtraction were used.

2.4. Catalyst activity

The activity testing was carried out in an isothermal fixed-bed reactor made of stainless steel (6 mm OD) at atmospheric pressure. The catalyst bed consisted of 100 mg of catalyst, pelletised and sieved to between 250 and 425 μm, placed between two plugs of quartz wool. Aera mass flow controllers were used to control the flow of Ar, CH_4, O_2/Ar and Ne to the reactor. Prior to the catalytic tests, each catalyst was oxidized under a flow of 5% O_2/Ar at a flow rate of 50 mL min^{-1} at 500 °C for 1 h with a heating rate 5 °C min^{-1}. The reaction gas mixture, which consisted of 27% CH_4, 13% O_2, 4% Ne and 56% Ar by volume, was then fed to the fixed bed reactor with the total flow maintained at 105 mL min^{-1}, giving a WHSV of 63,000 mL g^{-1} h^{-1}. The reaction temperature was measured using a thermocouple placed in the middle of the catalyst bed and the internal standard was 4% Ne in the feed. The products were analysed by on-line gas chromatography using a Perkin Elmer 500 GC equipped with a Thermal Conductivity Detector (TCD) and a Flame Ionisation Detector (FID) and using a Hayesep column. The conversion is that of methane relative to the internal standard and the selectivity is given as the concentration of the product relative to the total carbon containing products formed. See Scheme S1 (ESI) for details of calculations.

3. Results and discussion

3.1. Catalyst characterization

3.1.1. Surface area measurements

The surface areas and pore volumes, as measured by BET are given in Table 1 and the isotherms are shown in Fig. S1 (ESI). These were found to reflect the surface areas of the supports from which they were prepared with some influence of the preparation method. As expected the lower surface area η-Al_2O_3 (223 m^2 g^{-1}) [31] resulted in lower surface area catalysts than that of H-ZSM-5 (425 m^2 g^{-1}). The CeZr prepared by co-precipitation resulted in the lowest surface area although those prepared by co-precipitation showed higher surface areas and pore volumes than those prepared

Table 1
Effect of support and preparation method on the physical properties of the Ni catalysts prepared from alumina and ZSM-5 (80).

	Catalysts calcined at 550 °C		Catalysts calcined at 700 °C	
Catalyst abbreviation	S_{BET} area/($m^2\ g^{-1}$)	Pore Volume/($cm^3\ g^{-1}$)	S_{BET} area/($m^2\ g^{-1}$)	Pore Volume/($cm^3\ g^{-1}$)
η-Al_2O_3	223	0.5	180	0.39
H-ZSM-5(80)	425	0.17	406.3	0.16
$CeZr^{Com}$	47	0.07	–	–
NiAl	217	0.26	190.3	0.26
NiZ	341	0.08	330	0.077
NiCeZr-CP	99	0.11	74.7	0.098
NiCeZrAl-CP	199	0.40	169	0.38
NiCeZrAl-WI	159	0.23	139.3	0.22
NiCeZrZ-CP	309	0.16	304.6	0.16
NiCeZrZ-WI	254	0.09	250.2	0.09

by wet-impregnation for both alumina and ZSM-5 (80) supports. On further heating to the maximum reaction temperature of 700 °C the surface areas of all supports and catalysts decreased with the greater decrease of 20–30 $m^2\ g^{-1}$ observed with the η-Al_2O_3 catalysts compared with a decrease of 4–11 $m^2\ g^{-1}$ observed for H-ZSM-5 catalysts. It is noted that the η-Al_2O_3 does not undergo a phase change at the reaction temperatures [31].

3.1.2. X-ray diffraction (XRD) analysis

The diffractograms of the alumina and ZSM-5(80) zeolite catalysts are shown in Fig. 1a and Fig. 1b, respectively. Fig. 1a shows the XRD patterns of NiAl, NiCeZr-CP, NiCeZrAl-CP and NiCeZrAl-WI along with the η-Al_2O_3 and CeZr supports. The structure of η-Al_2O_3 was confirmed by the presence of diffraction lines at 2θ = 36, 45 and 66° (JCDD 04-0875) [31]. The $CeZrO_2$ diffractogram displayed diffraction lines at 2θ = 29.5, 33.1, 49.1, 58.5 and 79.5° corresponding to cerium zirconium oxide (JCPDS 38-1436) [32]. The diffractogram for the NiCeZrAl-CP catalyst showed low intensity peaks with no peaks observed for NiO indicating that the material was amorphous or that the NiO had an average particle size of less than the detection limit of the instrument. The same catalyst prepared on the lower surface area CeZrAl-WI support was more crystalline and showed peaks attributable to NiO at 2θ = 37, 43.1 and 62.4° indicating poor metal dispersion [14,15]. The lowest surface area support, CeZr-CP gave the highest intensity NiO peaks showing the inverse relationship between the available surface area of the support and the NiO particle size.

In the case of the ZSM-5(80) support (Fig. 1b), peaks attributable to NiO were observed in all cases. This may be due to the smaller pore volume of ZSM-5(80) compared to alumina (approximately 0.12 and 0.3 $cm^3\ g^{-1}$ respectively) meaning the accessible surface area for deposition of $CeZrO_2$ and Ni may be less than measured by BET resulting a lower dispersion than expected.

3.1.3. H_2-TPR and TPO

The H_2-TPR spectra for the alumina catalysts and zeolite catalysts are given in Fig. 2a and b, respectively. There were no reduction peaks for the η-Al_2O_3 and ZSM-5(80) supports in the temperature range from −20 °C to 700 °C [33] but a broad peak was observed at about 565 °C for CeZr [34]. On addition of Ni the reduction profile becomes more complicated with that of NiCeZr–CP showing a number of reduction regions. The increase in temperature of the NiO reduction peak and its overlap with the peak from Ce^{4+} reduction indicates complex interactions occurring between the metal and support. De Abreu et al. attributed the lower temperature peaks below 500 °C to the reduction of relatively free NiO species and surface Ce^{4+} in CeO_2 [14]. The presence of a broad and poorly defined peak at a temperature greater than 500 °C in samples containing alumina is attributed to reduction of NiO either strongly interacting with or incorporated into the alumina on preparation of the catalyst. These peaks are particularly prominent in the catalyst prepared by co-precipitation indicating very close interaction between all components [35].

The H_2-TPR spectra for the zeolite containing catalysts also show a range of features within one main broad peak indicating complex interactions between the metal and support components, Fig. 2b, with the peaks attributable to NiO being reduced at a slightly higher temperature than for the alumina based catalysts or the CeZr-CP single support. This may be due to the increased acidity of the zeolite increasing the electrophilicity of the nickel or the stronger interaction of the nickel with the support. In the case of NiZ, at least three main peaks are detected: a small peak at about 310 °C and a larger one with a shoulder between 345 and 530 °C. The lower temperature peak is attributed to bulk NiO on the zeolite whereas the higher temperature peak is associated with NiO reduction inside the channels of the ZSM-5 [36].

TPO analysis of the NiCeZrZ-CP catalyst is shown in Fig. S2 (ESI). An extremely broad peak ranging from 160 °C to almost 600 °C is observed showing many oxidation steps occurring during the oxidation of different sized nickel species in different chemical and physical environments [7]. Oxidation at lower temperatures is attributed to oxidation of smaller Ni particles [7,37].

TPR and TPO analysis shows the presence of a wide variety of nickel particles existing in differing chemical environments with the XRD analysis only showing larger crystalline particles. TEM analysis shown in Fig. S3 (ESI) of the NiCeZrZ-CP supports these observations with dark spots indicating the presence of nickel being distributed throughout the structure with particle sizes between 2 and 4 nm despite the presence of larger NiO being observed on the XRD.

3.1.4. DRIFTS-pyridine analysis

In-situ DRIFTS-pyridine analysis was performed on the two acidic supports that were used during the preparation of the catalysts as shown and discussed in Fig. S4 (ESI). As expected the H-ZSM-5 support showed a greater number of stronger acid sites than the η-Al_2O_3 and the catalysts prepared from these supports also showed the same trend. Fig. S5 (ESI) shows catalysts prepared from ZSM-5(80) having a higher number and strength of acid sites than those prepared from η-Al_2O_3 with NiCeZr-CP showing the least acidity among the series of the catalysts.

3.1.5. SEM and EDX analyses

Figs. S([0–9]) and S7 (ESI) show the SEM images of the catalysts used in this study. The NiAl and NiZ catalysts, prepared by wet impregnation showed very different morphologies with the alumina supported catalysts giving larger very smooth crystals compared to the smaller more uniform spherical crystals obtained from NiZ, consistent with the surface area results in Table 1. The catalysts containing CeZr prepared by wet impregnation largely

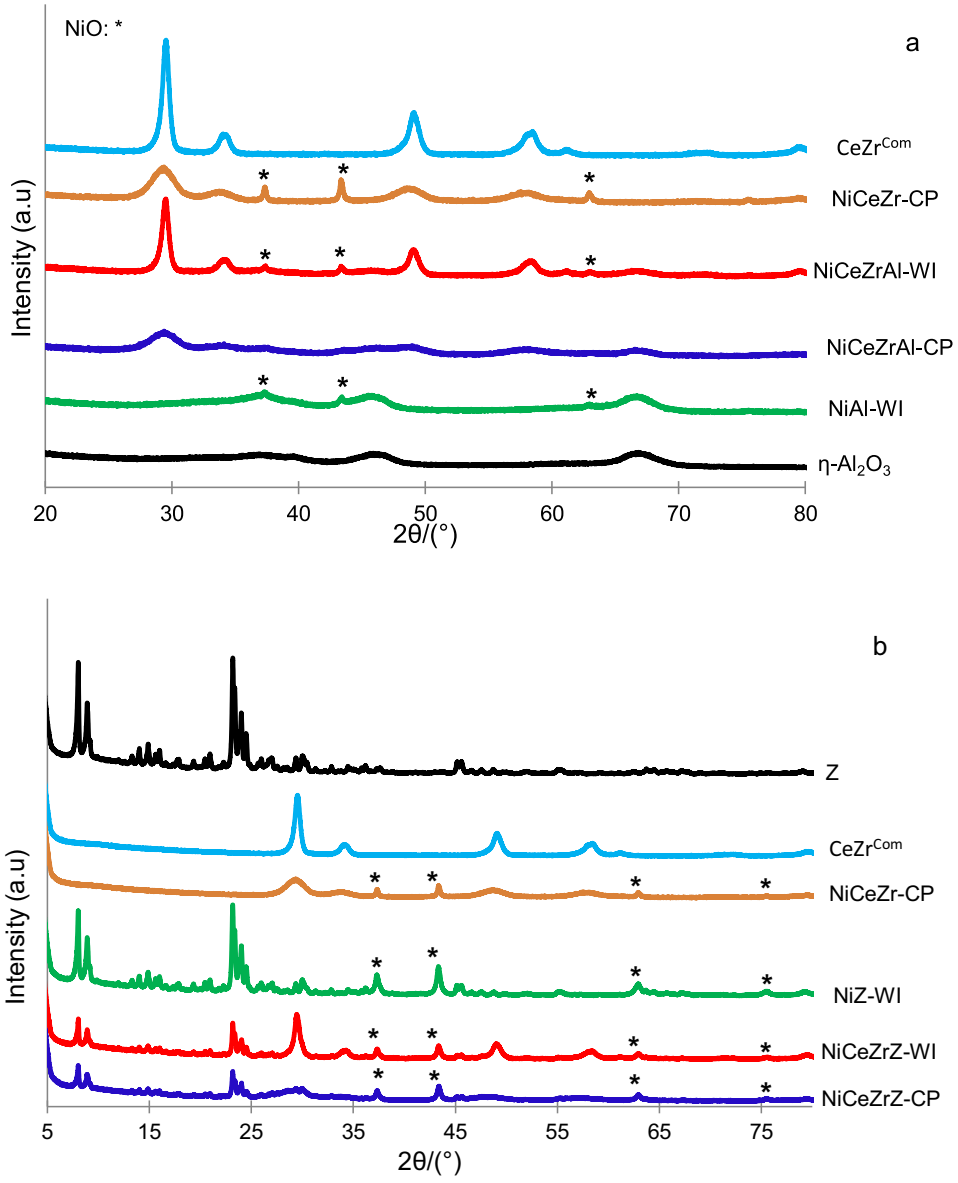

Fig. 1. XRD patterns of Ni catalysts supported on a) η-Al_2O_3, b) ZSM-5(80) that were prepared either by co-precipitation (CP) or wet-impregnation (WI). *Indicates NiO.

maintained these structures, however, the catalysts prepared by co-precipitation showed very different morphologies in each case. NiCeZrAl-CP did not show the larger smooth crystals observed in the previous two alumina catalysts, rather it was composed of smaller rougher crystals. Unlike the small regular crystals formed by the previous two zeolite catalysts, NiCeZrZ-CP was composed of small irregular crystals covered with a finer powder.

Table 2 and Fig. S8 (ESI) show the composition of the η-Al_2O_3 and ZSM-5 catalysts determined by EDX. Each catalyst contained 10 wt% Ni with the exception of NiCeZrAl-WI where it was lower at 7.3 wt%. This suggests that the metal dispersion of nickel is less homogeneous on this lower surface area support where areas of larger Ni particles are present, as shown in the XRDs in Fig. 1, along with areas of lower nickel loading.

Table 2
Composition of catalysts as determined from EDX/SEM analysis.

	Ni	Ce	Zr	O	Si	Al
NiAl	9.9	–	–	54.6	–	35.5
NiZ	10	–	–	55.3	33.8	0.9
NiCeZrAl-CP	10.7	9.7	6.9	43.9	–	28.8
NiCeZrAl-WI	7.3	4.2	2.7	50.4	–	35.4
NiCeZrZ-CP	10.3	9	5.7	50.7	23.5	0.7
NiCeZrZ-WI	10.2	11.4	5.9	43.7	27.8	1
NiCeZr-CP[a] (after reaction)	4.6	9.8	3.8	8.6	–	0.4
NiCeZrZ-CP (after reaction)	10.3	9	5.7	50.8	23.5	0.7

[a] The balance of 72.8% of this sample was detected as carbon.

3.1.6. XPS analysis

The XPS analysis for the NiCeZrZ-CP catalyst is shown in Fig. 3 with the composition obtained given in Table S1 (ESI). The Ni $2p_{3/2}$ spectrum (Fig. 3a) shows nickel to be predominantly present in the +2 oxidation state as a mixture of both NiO (854.2 eV) and $Ni(OH)_2$ (855.7 eV) with their satellite peak at ~861.5 eV [38–41]. There is however a minor contribution from metallic Ni at a binding energy ~852.5 eV. This is expected given the ease with which a Ni surface is passivated by oxygen. Fig. 3(a) also shows the Ce 3d spectrum which is complex. The component peak at 917 eV is a fingerprint of Ce^{4+} state and identifies the presence of CeO_2 which contributes to two sets of peaks at approximately 883, 889,

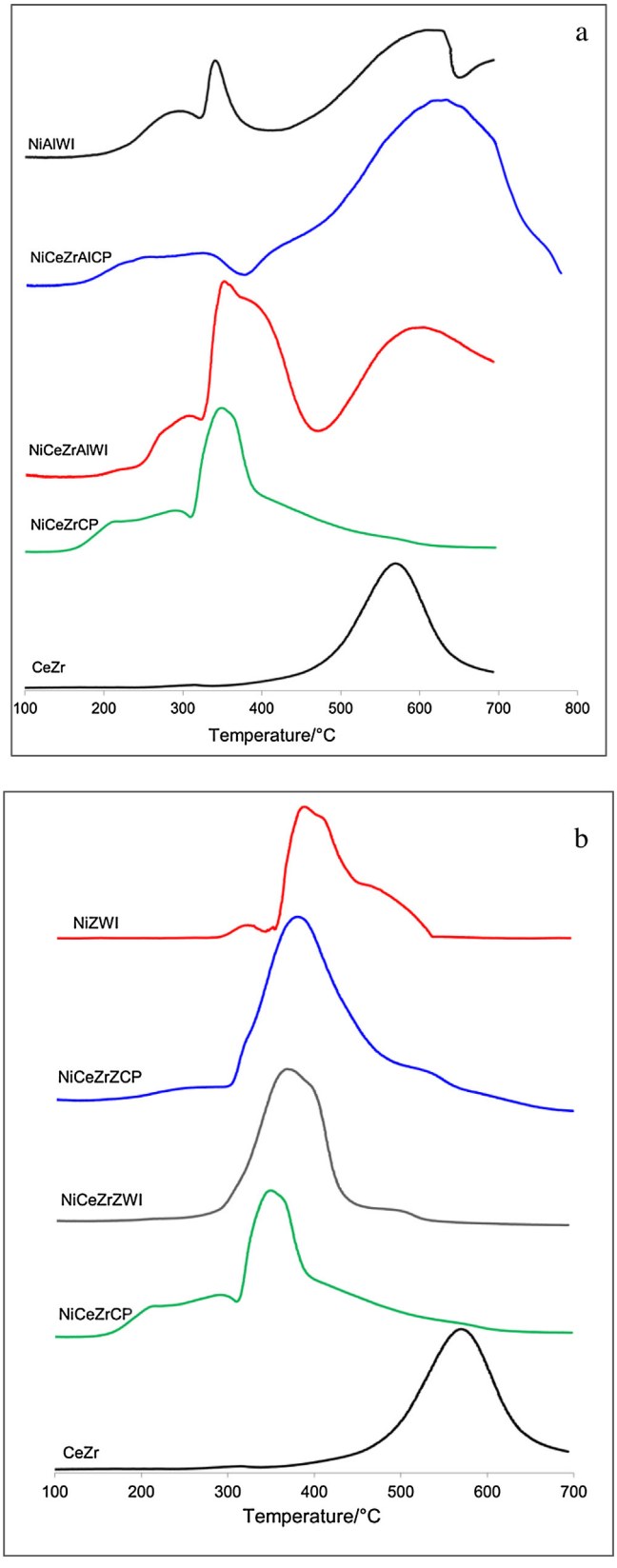

Fig. 2. H_2-TPR profile of Ni catalysts supported on a) η-Al_2O_3, b) ZSM-5 (80) prepared either by co-precipitation (CP) or wet-impregnation (WI).

899 eV (Ce$3d_{5/2}$) and 901, 908, 917 eV (Ce$3d_{3/2}$). [42,43]. However, additional peaks at 885 eV (Ce$3d_{5/2}$) and 904 eV (Ce$3d_{3/2}$) with indication of the second pair of spin orbit doublet at 880 eV (Ce$3d_{5/2}$) and 898 eV (Ce$3d_{3/2}$) are characteristic of a significant amount of Ce^{3+} [42]. The Zr 3d spectrum (Fig. 3b) is composed of a single doublet at 182.5 eV (Zr$3d_{5/2}$) and 184.9 eV (Zr$3d_{3/2}$) which is characteristic of zirconium present in its +4 oxidation state [44–46]. The O *1s* spectrum can be fitted with component peaks to show

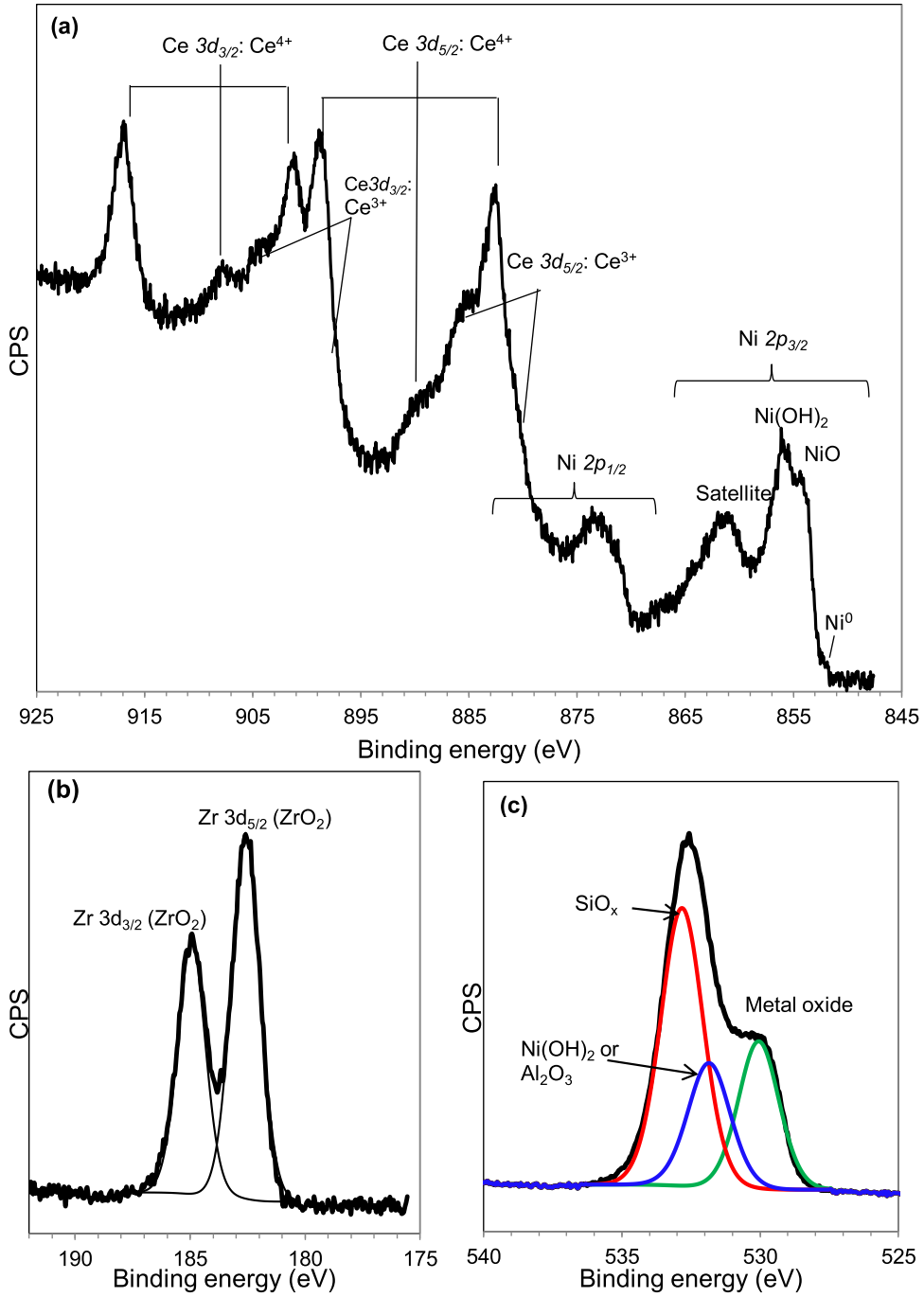

Fig. 3. XPS of (a) Ni*2p* and Ce*3d*, (b) Zr*3d* and (c) O*1s* regions for the NiCeZrZ-CP catalyst.

the presence of the related oxygens from the metal oxides (NiO, Ce oxides) at approximately 530 eV, $Ni(OH)_2/Al_2O_3$ at 531.5 eV and SiO_x at 533 eV.

3.2. Catalyst activity

3.2.1. General kinetic data

The products observed in the outlet stream of the reactor by GC analysis were mainly CO and H_2 with a small proportion being CO_2 and H_2O confirming that at temperatures greater than 600 °C the main reaction was CPOM. In all cases, a carbon balance greater than 99% was obtained and no reaction occurred at 300 °C.

The conversion of methane at various reaction temperatures is given in Fig. 4 and the temperatures required to reach 50%, 70% and 90% conversion ($T_{50\%}$, $T_{70\%}$ and $T_{90\%}$ respectively) for each catalyst are summarised in Table 3.

Table 3
The temperature required to reach 50%, 70% and 90% conversion using catalysts prepared on η-Al_2O_3, ZSM-5(80) and CeZr-CP with different preparation methods.

Catalyst	$T_{50\%}$ (°C)	$T_{70\%}$ (°C)	$T_{90\%}$ (°C)
NiAl	482	570	760
NiZ	455	555	719
NiCeZr-CP	465	558	725
NiCeZrAl-CP	425	540	708
NiCeZrAl-WI	440	550	715
NiCeZrZ-CP	392	515	690
NiCeZrZ-WI	415	530	705

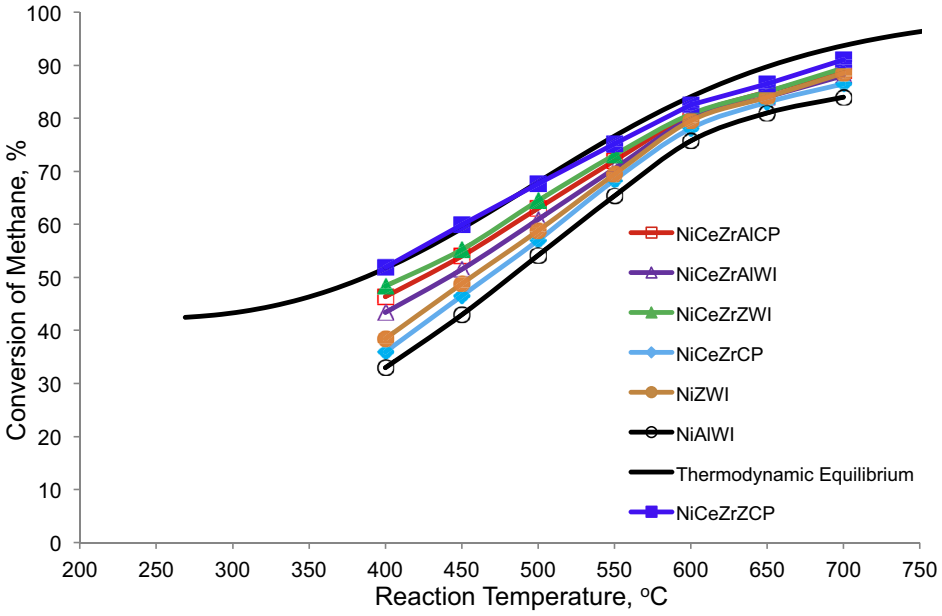

Fig. 4. Catalytic activity of the Ni catalysts prepared on η-Al_2O_3, ZSM-5(80) and CeZr-CP with different preparation methods at temperatures between 400 and 750 °C and a WHSV of 63,000 mL g^{-1} h^{-1}.

There was no reaction at 300 °C even for the most active NiCeZrZ-CP catalyst but once the reaction started at 400 °C it occurred rapidly with the conversion almost reaching equilibrium. From the TPO in Fig. S2 (ESI) many of the smaller Ni particles are easily oxidized at temperatures below 300 °C. As such the rapid onset of the CPOM reaction above 400 °C is here attributed to the reduction of NiO in agreement with the TPR analysis in Fig. 2. The generally high activity of these catalysts and NiCeZrZ-CP in particular is due to the close interaction of all catalyst components which allows for their facile redox behaviour. XPS analysis shows the presence of cerium in both the +3 and +4 oxidation states indicating a ready exchange between oxidation states and facile oxygen transfer to the Ni active site. Similarly, the presence of Ni as the metal, oxide and hydroxide indicates a ready exchange between oxidation states as required for this oxidation reaction.

For reactions over catalysts with a single acidic support, NiAl and NiZ the zeolite was the most active giving a $T_{50\%}$ of 455 °C compared with 482 °C for NiAl. Despite its very low surface area of 99 m^2 g^{-1} compared with 341 m^2 g^{-1} and 217 m^2 g^{-1} for NiZ and NiAl respectively the NiCeZr-CP is more active than NiAl with a $T_{50\%}$ of 465 °C. Therefore, as expected the support influences the activity of the catalyst which is not simply dependent on the support surface area. The higher activity of the catalysts prepared on the zeolite supports is reflected in catalysts prepared with CeZr added. Regardless of the preparation method, the zeolite catalysts were more active than the equivalent catalyst prepared with η-Al_2O_3 with $T_{50\%}$ of 392 and 415 °C for NiCeZrZ-CP and NiCeZrZ-WI respectively compared with 425 °C and 440 °C for NiCeZrAl-CP and NiCeZrAl-WI respectively. This could be due to a number of reasons such as increased interaction between the Ni and the zeolite based support as evidenced by the increased reduction temperature observed by TPR. Despite the presence of larger NiO particles observed in the X-ray diffractograms of the zeolite based catalysts, the larger surface area pore structure of the zeolite may result in a proportionally larger number of smaller nickel particles and higher dispersion in the pores. The increased interaction and interfacial area between the nickel and the support would allow improved transport of the oxygen from the CeZr in the support onto the nickel for its reoxidation and also removal of any coke that may be deposited. In addition, the increased acidity of the zeolite compared with the η-Al_2O_3, as shown in the pyridine DRIFTS experiments, may increase the electrophilicity of the nickel improving the reoxidation step in the catalytic cycle resulting in a faster reaction. Alternatively, the very strongly adsorbed nickel species on alumina based catalysts, indicated in the TPR analysis which may in fact be incorporated into the support, could restrict availability of the nickel for catalysis making the η-Al_2O_3 catalysts less active.

Comparison of the method of preparation for the zeolite catalysts shows that catalysts prepared by co-precipitation are more active than those prepared by wet-impregnation. This higher activity is attributed to improved interaction between the three phases of the catalyst as indicated by the increase in temperature of reduction shown in the TPR analysis. A similar comparison for the η-Al_2O_3 catalysts is more difficult due to the more amorphous nature of the NiCeZrAl-CP catalyst as shown in the XRD and the strong interaction or incorporation of the nickel into the support.

In all cases, the selectivity to CO and H_2 increased with increasing temperature as shown in Fig. 5 with less than 5% methane converted to CO_2 at 700 °C. There was little difference in the observed selectivity between the catalysts and the H_2:CO ratio ranged between 1.5 at lower temperatures, increasing to 2 at 700 °C.

3.2.2. *Mass transfer limitations*

The change in gradient of the conversion against temperature graph at 600 °C shown in Fig. 4 indicates that the observed kinetics may be under different limitations at different temperatures and so possible mass transfer limitations were tested. To evaluate the influence of diffusional limitation, the effect of particle size was examined and to assess mass transfer limitation by adsorption or desorption the activation energy of the reaction was calculated.

To examine the effects of diffusion, reactions were carried out over the most active catalyst, NiCeZrZ-CP using 250–425 μm pellets or a fine powder. The conversion of methane over the different sizes of catalyst particles at different temperatures is shown in Fig. S9 (ESI). As the rates of reaction were identical the reaction is not controlled by the particle size of the catalyst and, therefore, is not limited by diffusion through the catalyst pellet.

To examine the effects of adsorption/desorption, reactions were again carried out over NiCeZrZ-CP at different temperatures. The rate of reaction described in Eq. (1) below was combined with the

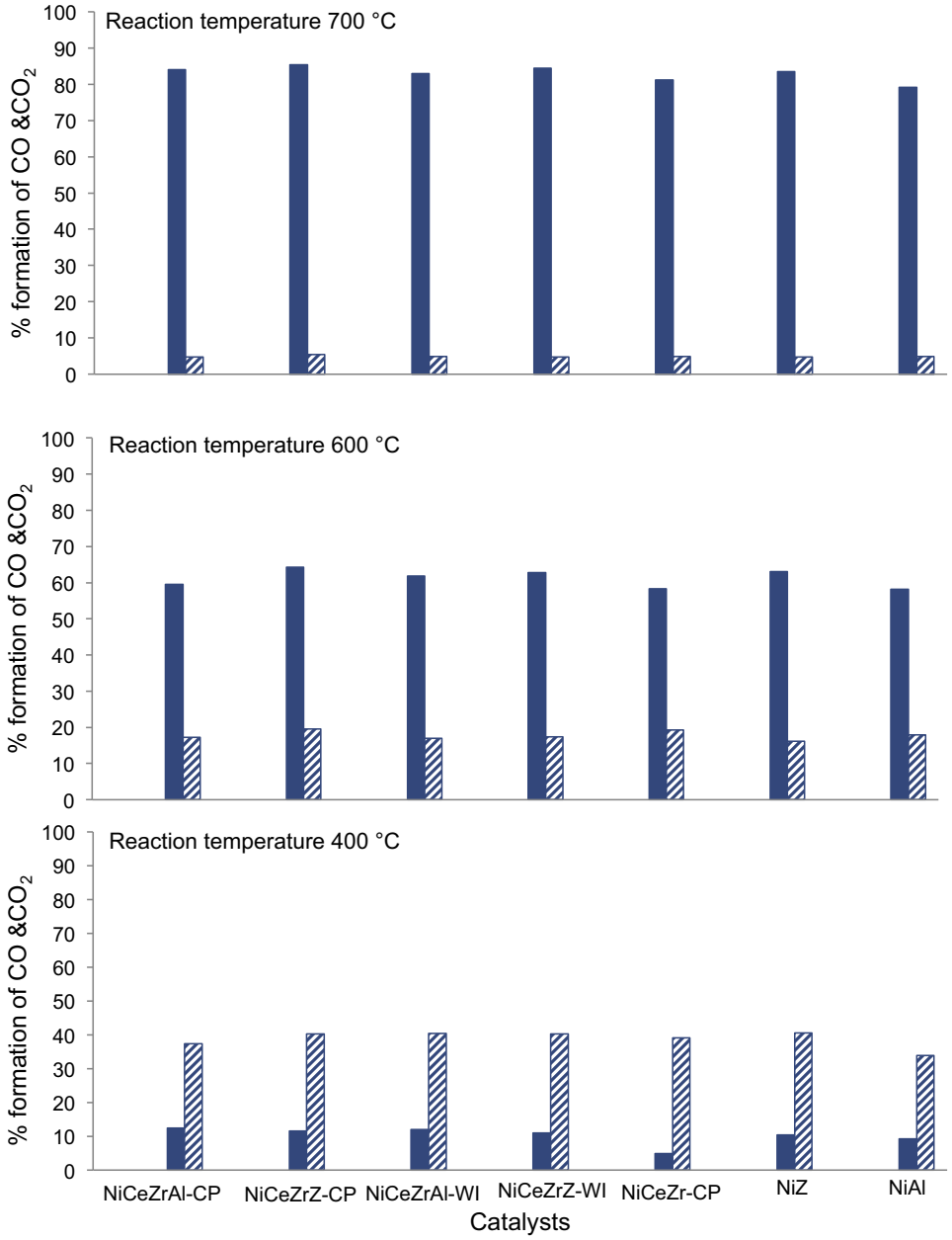

Fig. 5. Formation of CO (solid) and CO_2 (lined) over Ni catalysts prepared on η-Al_2O_3, ZSM-5(80) and CeZr-CP with different preparation methods at 400 °C (bottom), 600 °C (middle) and 700 °C (top). Reactions were carried out under reaction temperatures of between 400 and 700 °C with a WHSV of 63,000 mL g^{-1} h^{-1}.

Arrhenius Equation given in Eq. (2) to give an expression allowing estimation of the apparent activation energy E_a Eq. (3) [47].

$$r = k[CH_4]^m.[O_2]^n \quad (1)$$

$$k = k_0 \exp(-E_a/\mathrm{RT}) \quad (2)$$

$$\ln r = \ln k_0 + \frac{-E_a}{R} \cdot \frac{1}{T} + m\ln[CH_4] + n\ln[O_2] \quad (3)$$

Where r represents the reaction rate (mol g^{-1} s^{-1}), k is the rate constant, k_0 is the pre-exponential factor, R is the gas constant (8.314 J K^{-1} mol^{-1}), E_a is the apparent activation energy (J mol^{-1}), T is the temperature (K), and (m, n) represent the reaction order with respect to methane and oxygen, respectively. As oxygen is not present in excess n is not zero. The calculated apparent activation energies for the reaction between 400 °C and 600 °C and for reaction between 600 °C and 700 °C are summarised in Table 4.

Table 4
Activation Energies calculated from 400 to 700 °C for different catalysts.

Catalysts	E_a (400–600 °C)	E_a (600–700 °C)	E_a (400–700 °C)
NiAl	17.57	7.30	15.46
NiZ	17.74	7.54	17.57
NiCeZr-CP	19.03	7.24	16.36
NiCeZrAl-CP	13.48	7.90	12.30
NiCeZrAl-WI	15.03	6.82	13.36
NiCeZrZ-CP	11.29	6.90	10.30
NiCeZrZ-WI	12.78	7.24	11.60

Otsuka et al. reported a value of 71 kJ mol^{-1} for a stoichiometric CPOM reaction over a $Ce_{0.8}Zr_{0.2}O_2$ catalyst [34] which is clearly much higher than the values calculated herein. However, it should be noted that the apparent activation energy for NiCeZrZ-CP under differential conditions, at a conversion of less than 20% was found to be 64 kJ mol^{-1} which is in good agreement with

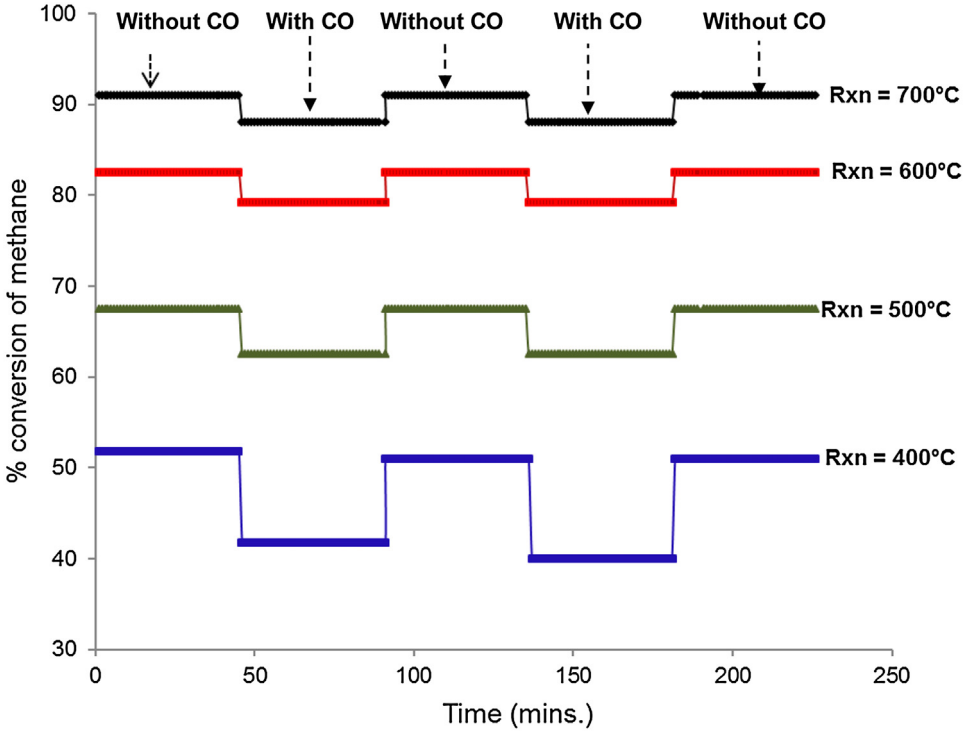

Fig. 6. The effect of addition of 5% CO to the feed for CPOM reaction over the NiCeZrZ-CP catalyst. Reaction conditions: temperature, 400–700 °C with WHSV, 63000 mL g^{-1} h^{-1}.

Fleys et al. [48] who quoted 54.4 kJ mol^{-1} under similar conditions.

It is well known that adsorption and desorption processes have an apparent activation energy of less than 20 kJ mol^{-1} [49] which in the case of the catalysts herein indicates that the observed kinetics are likely controlled by an adsorption or desorption step in the reaction. It is also known that nickel catalysts are susceptible to poisoning by strong adsorption of CO so 5% CO was periodically added to the inlet stream passed over NiCeZrZ-CP at temperatures between 400 and 700 °C and the effect on the observed kinetics monitored.

The square profile obtained, Fig. 6, shows that a decrease in catalyst activity is observed on addition of CO to the feed and that the extent of the decrease is greater at lower temperatures where the adsorption strength of the CO is greater. For the reaction carried out at 400 °C the conversion of methane decreased by 10% from 51.8% to 41.8% whereas when the reaction temperature was 700 °C the conversion only decreased by 3% from 91% to 88%. The deactivation was not permanent and when the CO was removed from the feed the activity of the catalyst immediately returned to its initial level.

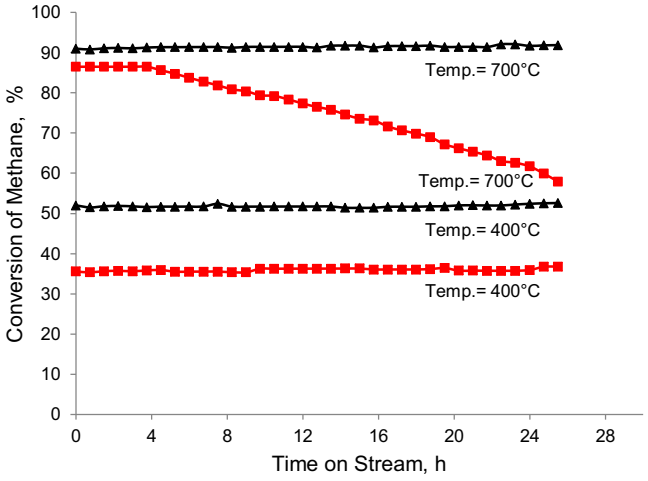

Fig. 7. Comparison of the stability of NiCeZrZ-CP (▲) and NiCeZr-CP (■) both prepared by co-precipitation. Reaction conditions: temperature, 700 °C and 400 °C for 25 h; WHSV, 63000 mL g^{-1} h^{-1}.

3.2.3. *Catalyst stability*

It is reported that although preparing catalysts by co-precipitation can improve the stability of the catalyst for the CPOM reaction, increased time on stream can still lead to deactivation [6,14,16]. This is often by coke formation or sintering of the metal which is common at the high temperatures required for reaction [50]. Ding et al. reported that nickel catalysts deactivate mainly by coke deposition [23]. To examine any deactivation effects, the catalysts were run under continuous operation at high (700 °C) and lower (400 °C) temperature. Fig. 7 shows that no deactivation occurred for NiCeZrZ-CP at either 700 °C or 400 °C over 25 h time on stream.

The equilibrium deactivation observed over the NiCeZrZ-CP means that although a temperature dependent steady state coverage of CO is maintained throughout the reaction, the catalyst is not permanently poisoned by the presence of CO but its activity is inhibited. Therefore, the catalysts are still active albeit at a reduced level for long time on stream.

However, at temperatures nearer 700 °C where coke formation is thermodynamically favourable a difference in stability is seen between the catalysts. Again, the reaction over NiCeZrZ-CP was stable for 25 h on stream and analysis of the spent catalyst by EDX/SEM did not detect the presence of any carbon. However, in the case of NiCeZr-CP, where the dispersion of the nickel particles is thought to be low and their interaction with the support weaker as shown by the lower temperature reduction peak, the deactivation of the catalyst occurs after only 4 h. An increase in pressure of the reactor to 2 bar was observed after 25.5 h reaction time and with a high proportion of carbon observed on the EDX analysis of the spent catalyst,

Table 2 and Fig. S8, this deactivation is attributed to coke formation. In this case, the lower surface area CeZr-CP is thought to result in a higher number of larger Ni particles as evidenced by the XRD analysis. In contrast, the higher surface area NiCeZrZ-CP is thought to show a higher dispersion of nickel, allowing a high interfacial area between the nickel and the support. This not only allows good interaction of the metal with the oxygen carrier during the reaction to improve the redox behaviour of the Ni but also allows easy transfer of oxygen to remove any coke which may deposit. Therefore, the larger particles on the CeZr-CP are more easily poisoned by carbon deposition at higher temperatures resulting in a rapid loss of activity.

4. Conclusions

A range of catalysts using Ni supported on an acidic support enhanced by an oxygen carrier has been shown to facilitate CPOM at low temperatures. Of the catalysts tested the best was a 10 wt% Ni on 25% CeO_2-ZrO_2/ZSM-5(80) prepared by co-precipitation giving near equilibrium conversion at 400 °C. The catalyst preparation method was shown to play an important role in the performance of the catalyst with co-precipitation producing a catalyst with a high surface area and pore volume and with good dispersion of the metal on the support. The high dispersion of the metal with the resulting high interfacial area between the metal and strong interaction of the Ni with the oxygen carrier improves the redox cycle of the Ni and also improves the supply of oxygen to remove carbon deposition at higher temperatures giving a highly active and stable catalyst.

Acknowledgements

The authors would like to acknowledge the support given to AO from South Valley University in Egypt and the group in Harbin for assistance in running TPO analysis. This publication was made possible by a NPRP grant from the Qatar National Research Fund (a member of The Qatar Foundation). The statements made herein are solely the responsibility of the authors.

Appendix A. Supplementary data

Supplementary data associated with this article can be found, in the online version, at http://dx.doi.org/10.1016/j.apcatb.2016.12.058.

References

[1] R. Horn, R. Schlogl, Methane activation by heterogeneous catalysis, Catal. Lett. 145 (2015) 23–39.
[2] P. Weiland, Biogas production: current state and perspectives, Appl. Microbiol. Biotechnol. 85 (2010) 849–860.
[3] Center for Climate and Energy Solutions, Leveraging Natural Gas to Reduce Greenhouse Gas Emissions, 2013.
[4] V.N. Nguyen, L. Blum, Syngas and synfuels from H_2O and CO_2: current status, Chem. Ing. Tech. 87 (2015) 354–375.
[5] B. Christian Enger, R. Lodeng, A. Holmen, A review of catalytic partial oxidation of methane to synthesis gas with emphasis on reaction mechanisms over transition metal catalysts, Appl. Catal. A: Gen. 346 (2008) 1–27.
[6] G. Pantaleo, V. La Parola, F. Deganello, P. Calatozzo, R. Bal, A.M. Venezia, Synthesis and support composition effects on CH_4 partial oxidation over Ni-CeLa oxides, Appl. Catal. B: Environ. 164 (2015) 135–143.
[7] J.A. Velasco, C. Fernandez, L. Lopez, S. Cabrera, M. Boutonnet, S. Jaras, Catalytic partial oxidation of methane over nickel and ruthenium based catalysts under low O_2/CH_4 ratios and with addition of steam, Fuel 153 (2015) 192–201.
[8] J. Kagawa, Health effects of diesel exhaust emissions—a mixture of air pollutants of worldwide concern, Toxicology 181–182 (2002) 349–353.
[9] S.A. Al-Sayari, Recent developments in the partial oxidation of methane to syngas, Open Catal. J. 6 (2013) 17–28.
[10] A.C.W. Koh, L. Chen, W. Kee Leong, B.F.G. Johnson, T. Khimyak, J. Lin, Hydrogen or synthesis gas production via the partial oxidation of methane over supported nickel–cobalt catalysts, Int. J. Hydrogen Energy 32 (2007) 725–730.
[11] E.C. Faria, R.C.R. Neto, R.C. Colman, F.B. Noronha, Hydrogen production through CO_2 reforming of methane over Ni/$CeZrO_2$/Al_2O_3 catalysts, Catal. Today 228 (2014) 138–144.
[12] W.-S. Dong, H.-S. Roh, K.-W. Jun, S.-E. Park, Y.-S. Oh, Methane reforming over Ni/Ce-ZrO_2 catalysts: effect of nickel content, Appl. Catal. A: Gen. 226 (2002) 63–72.
[13] A. Scarabello, D. Dalle Nogare, P. Canu, R. Lanza, Partial oxidation of methane on Rh/ZrO_2 and Rh/Ce-ZrO_2 on monoliths: catalyst restructuring at reaction conditions, Appl. Catal. B: Environ. 174–175 (2015) 308–322.
[14] A.J. de Abreu, A.F. Lucredio, E.M. Assaf, Ni catalyst on mixed support of CeO_2-ZrO_2 and Al_2O_3: Effect of composition of CeO_2-ZrO_2 solid solution on the methane steam reforming reaction, Fuel Process. Technol. 102 (2012) 140–145.
[15] T. Mondal, K.K. Pant, A.K. Dalai, Catalytic oxidative steam reforming of bio-ethanol for hydrogen production over Rh promoted Ni/CeO_2-ZrO_2 catalyst, Int. J. Hydrogen Energy 40 (2015) 2529–2544.
[16] M. Dajiang, C. Yaoqiang, Z. Junbo, W. Zhenling, M. Di, G. Maochu, Catalytic partial oxidation of methane over Ni/CeO_2 −ZrO_2 −Al_2O_3, J. Rare Earths 25 (2007) 311–315.
[17] S. Xu, X. Wang, Highly active and coking resistant Ni/CeO_2–ZrO_2 catalyst for partial oxidation of methane, Fuel 84 (2005) 563–567.
[18] X. Cai, Y. Cai, W. Lin, Autothermal reforming of methane over Ni catalysts supported over ZrO2-CeO2-Al2O3, J. Nat. Gas Chem. 17 (2008) 201–207.
[19] A.S. Larimi, S.M. Alavi, Ceria-Zirconia supported Ni catalysts for partial oxidation of methane to synthesis gas, Fuel 102 (2012) 366–371.
[20] R. Jin, Y. Chen, W. Li, W. Cui, Y. Ji, C. Yu, Y. Jiang, Mechanism for catalytic partial oxidation of methane to syngas over a Ni/Al_2O_3 catalyst, Appl. Catal. A: Gen. 201 (2000) 71–80.
[21] R. Lanza, P. Canu, S.G. Jaras, Methane partial oxidation over Pt–Ru catalyst: an investigation on the mechanism, Appl. Catal. A: Gen. 375 (2010) 92–100.
[22] A.G. Steghuis, J.G. van Ommen, J.A. Lercher, On the reaction mechanism for methane partial oxidation over yttria/zirconia, Catal. Today 46 (1998) 91–97.
[23] C. Ding, J. Wang, Y. Jia, G. Ai, S. Liu, P. Liu, K. Zhang, Y. Han, X. Ma, Anti-coking of Yb-promoted Ni/Al_2O_3 catalyst in partial oxidation of methane, Int. J. Hydrogen Energy 41 (2016) 10707–10718.
[24] D.A. Hickman, L.D. Schmidt, Synthesis gas formation by direct oxidation of methane over Pt monoliths, J. Catal. 138 (1992) 267–282.
[25] R. Horn, K.A. Williams, N.J. Degenstein, L.D. Schmidt, Syngas by catalytic partial oxidation of methane on rhodium: mechanistic conclusions from spatially resolved measurements and numerical simulations, J. Catal. 242 (2006) 92–102.
[26] R. Horn, K.A. Williams, N.J. Degenstein, A. Bitsch-Larsen, D. Dalle Nogare, S.A. Tupy, L.D. Schmidt, Methane catalytic partial oxidation on autothermal Rh and Pt foam catalysts: oxidation and reforming zones, transport effects, and approach to thermodynamic equilibrium, J. Catal. 249 (2007) 380–393.
[27] W.Z. Weng, M.S. Chen, Q.G. Yan, T.H. Wu, Z.S. Chao, Y.Y. Liao, H.L. Wan, Mechanistic study of partial oxidation of methane to synthesis gas over supported rhodium and ruthenium catalysts using in situ time-resolved FTIR spectroscopy, Catal. Today 63 (2000) 317–326.
[28] J.N. Carstens, S.C. Su, A.T. Bell, Factors affecting the catalytic activity of Pd/ZrO_2 for the combustion of methane, J. Catal. 176 (1998) 136–142.
[29] A.I. Osman, J.K. Abu-Dahrieh, F. Laffir, T. Curtin, J.M. Thompson, D.W. Rooney, A bimetallic catalyst on a dual component support for low temperature total methane oxidation, Appl. Catal. B: Environ. 187 (2016) 408–418.
[30] K.A. Chalupka, W.K. Jozwiak, J. Rynkowski, W. Maniukiewicz, S. Casale, S. Dzwigaj, Partial oxidation of methane on NixAlBEA and NixSiBEA zeolite catalysts: remarkable effect of preparation procedure and Ni content, Appl. Catal. B: Environ. 146 (2014) 227–236.
[31] A.I. Osman, J.K. Abu-Dahrieh, D.W. Rooney, S.A. Halawy, M.A. Mohamed, A. Abdelkader, Effect of precursor on the performance of alumina for the dehydration of methanol to dimethyl ether, Appl. Catal. B: Environ. 127 (2012) 307–315.
[32] B. Zhao, C. Huang, R. Ran, X. Wu, D. Weng, Two-step thermochemical looping using modified ceria-based materials for splitting CO_2, J. Mater. Sci. 51 (2015) 2299–2306.
[33] Y.-S. Bi, G.-Y. Dang, X.-H. Zhao, X.-F. Meng, H.-J. Lu, J.-T. Jin, Preparation characterization and catalytic properties of Pd-Fe-zeolite and Pd-Ce-zeolite composite catalysts, J. Hazard. Mater. 229–230 (2012) 245–250.
[34] K. Otsuka, Y. Wang, M. Nakamura, Direct conversion of methane to synthesis gas through gas-solid reaction using CeO_2-ZrO_2 solid solution at moderate temperature, Appl. Catal. A: Gen. 183 (1999) 317–324.
[35] J.S. Lisboa, L.E. Terra, P.R.J. Silva, H. Saitovitch, F.B. Passos, Investigation of Ni/Ce-ZrO_2 catalysts in the autothermal reforming of methane, Fuel Process. Technol. 92 (2016) 2075–2082.
[36] B. Sarkar, R. Tiwari, R.K. Singha, S. Suman, S. Ghosh, S.S. Acharyya, K. Mantri, L.N.S. Konathala, C. Pendem, R. Bal, Reforming of methane with CO_2 over Ni nanoparticle supported on mesoporous ZSM-5, Catal. Today 198 (2012) 209–214.
[37] F. Basile, P. Benito, G. Fornasari, D. Gazzoli, I. Pettiti, V. Rosetti, A. Vaccari, Ni-catalysts obtained from silicate intercalated HTlcs active in the catalytic partial oxidation of methane: influence of the silicate content, Catal. Today 142 (2009) 78–84.
[38] M. Lenglet, F. Hochu, J. Dürr, M.H. Tuilier, Investigation of the chemical bonding in 3d8 nickel(II) charge transfer insulators (NiO, oxidic spinels) from ligand-field spectroscopy Ni 2p XPS and X-ray absorption spectroscopy, Solid State Commun. 104 (1997) 793–798.

[39] A.P. Grosvenor, M.C. Biesinger, R.S.C. Smart, N.S. McIntyre, New interpretations of XPS spectra of nickel metal and oxides, Surf. Sci. 600 (2006) 1771–1779.
[40] L.J. Mantienzo, L. Yin, S.O. Grim, W.E. Swartz, X-ray photoelectron spectroscopy of nickel compounds, Inorg. Chem. 12 (1973) 2763–2769.
[41] W.H. Nesbitt, D. Legrand, M.G. Bancroft, Interpretation of Ni2p XPS spectra of Ni conductors and Ni insulators, Phys. Chem. Miner. 27 (2000) 357–366.
[42] X. Yao, C. Tang, Z. Ji, Y. Dai, Y. Cao, F. Gao, L. Dong, Y. Chen, Investigation of the physicochemical properties and catalytic activities of $Ce_{0.67}M_{0.33}O_2$ ($M = Zr^{4+}$, Ti^{4+} Sn^{4+}) solid solutions for NO removal by CO, Catal. Sci. Technol. 3 (2013) 688–698.
[43] C. Zhang, J. Lin, Visible-light induced oxo-bridged ZrIV-O-CeIII redox centre in tetragonal ZrO_2-CeO_2 solid solution for degradation of organic pollutants, Phys. Chem. Chem. Phys. 13 (2011) 3896–3905.
[44] S.V. Ketov, X. Shi, G. Xie, R. Kumashiro, A.Y. Churyumov, A.I. Bazlov, N. Chen, Y. Ishikawa, N. Asao, H. Wu, D.V. Louzguine-Luzgin, Nanostructured Zr-Pd metallic glass thin film for biochemical applications, Sci. Rep. 5 (2015) 1–7, 7799.
[45] C.-C. Wu, C.-K. Wei, C.-C. Ho, S.-J. Ding, Enhanced hydrophilicity and biocompatibility of dental zirconia ceramics by oxygen plasma treatment, Materials 8 (2015) 684–699.
[46] B.-G. Son, S.Y. Je, H.J. Kim, J.K. Jeong, Modification of a polymer gate insulator by zirconium oxide doping for low temperature, high performance indium zinc oxide transistors, RSC Adv. 4 (2014) 45742–45748.
[47] H. Geng, Z. Yang, L. Zhang, J. Ran, Y. Chen, Experimental and kinetic study of methane combustion with water over copper catalyst at low-temperature, Energy Convers. Manag. 103 (2015) 244–250.
[48] M. Fleys, W. Shan, Y. Simon, P.-M. Marquaire, Detailed kinetic study of the partial oxidation of methane over La_2O_3 catalyst. Part 1: experimental results, Ind. Eng. Chem. Res. 46 (2007) 1063–1068.
[49] A.W. Harding, N.J. Foley, P.R. Norman, D.C. Francis, K.M. Thomas, Diffusion barriers in the kinetics of water vapor adsorption/desorption on activated carbons, Langmuir 14 (1998) 3858–3864.
[50] C.H. Bartholomew, Mechanisms of catalyst deactivation, Appl. Catal. A: Gen. 212 (2001) 17–60.